Importance of Tidal Stress in the Numerical Model of Residual Flow in the Coastal Sea

Yanagi, Tetsuo
Research Institute for Applied Mechanics, Kyushu University

Yamamoto, Jun
Department of Civil and Environmental Engineering, Ehime University

Morimoto, Akihiko
Department of Civil and Environmental Engineering, Ehime University

Fujihara, Masayuki
College of Agriculture, Ehime University

https://doi.org/10.5109/6786352

出版情報：Reports of Research Institute for Applied Mechanics. 44 (116), pp.1-10, 1998-10. 九州大学応用力学研究所

Importance of Tidal Stress in the Numerical Model of Residual Flow in the Coastal Sea

By Tetsuo YANAGI*[1], Jun YAMAMOTO*[2], Akihiko MORIMOTO*[2] and Masayuki FUJIHARA*[3]

Result of residual flow calculation in the coastal sea by the diagnostic numerical model with the tidal stress, which is due to the nonlinear effect of tidal current, and that without the tidal stress are compared to the field observation result of residual flow by HF radar in Bungo Channel, Japan. Comparison shows that it is essentially important to include the tidal stress in the diagnostic numerical calculation of residual flow in the coastal sea where tidal current is dominant.

Key Words: Tidal stress, residual flow, numerical model, coastal sea

1. Introduction

Usually, the tidal current is the most dominant current and the residual flow, which is the averaged flow over one tidal cycle, is very weak compared to the tidal current in the coastal sea. However, the residual flow plays more important role than the tidal current in the long term material transport in the coastal sea. The comprehensive coastal circulation models have been developed (e.g. Backhaus and Hain Buche, 1987 [1], Blumberg and Mellor, 1987 [2], Pohlmann, 1996 [3], Lynch et al., 1996 [4]) and the tidal current and the residual flow are calculated at the same time in their models. The main components of residual flow in the coastal sea are the wind-driven current, the density-driven current and the tide-induced residual flow and their time scales of temporal variation are completely different from that of tidal current. The tidal current does not change temporally without the spring-neap modulation but the temporal variability of residual flow is very large due to the large variability of wind, fresh water discharge, heat transfer through the sea surface and so on. Therefore it is wiqser to calculate separately the tidal current and the residual flow in the numerical model from the economical viewpoint of computational time.

We have to include theoretically the tidal stress in the diagnostic or prognostic numerical calculation of residual flow in the case where we do not directly calculate tidal current field in the coastal sea. However, there has been no study on the necessity or importance of including tidal stress in the diagnostic or prognostic numerical calculation of residual flow in the coastal sea so far. This is mainly due to the lack of adequate observational data of residual flow in the coastal sea for the verification of model result. We could not decide which is more accurate numerical calculation with the tidal stress or without the tidal stress because we did not have adequate obsevational data to verify the model result. Yanagi et al. (1994) [5] obtained the horizontal distribution of surface residual flow in Bungo Channel, Japan with use of HF (High Frequency) radar.

We will develop two kinds of diagnostic numerical models for the calculation of residual flow in the coastal sea, that is, one with the tidal stress and another without the tidal stress. We will compare both calculation results of residual flow by two models with that of field observation result by HF radar in Bungo Channel in this paper.

*1 Research Institute for Applied Mechanics, Kyushu University
*2 Department of Civil and Environmental Engineering, Ehime University
*3 College of Agriculture, Ehime University

2. Field observation

Field observation of residual flow with use of HF radar was carried out from 18 June 1992 to 28 June

1992 in Bungo Channel, the western part of the Seto Inland Sea, Japan (Fig.1). Two HF radars were set at Seto and Oohama in Fig.1 and surface currents at 70 points in Bungo Channel were observed every 2 hours during 9 days from 19 June to 27 June 1992. The day-to-day variation of residual flow field, which was obtained by averaging observed current over 24 hours, was very small (Yanagi et al., 1994) [5] and the residual flow field averaged over 9 days was obtained, which will be shown later in Fig.9 (a). We want to reproduce this residual flow field by the diagnostic numerical calculation.

3. Numerical model

3.1 Tide, tidal current and tide-induced residual flow

At first, the tide and tidal current in Bungo Channel are reproduced. The governing equations of tide and three-dimensional tidal current are as follows.

$$\frac{\partial u}{\partial t}+u\frac{\partial u}{\partial x}+v\frac{\partial u}{\partial y}+w\frac{\partial u}{\partial z}-fv =-g\frac{\partial \eta}{\partial x}+\nu_h\left(\frac{\partial^2 u}{\partial x^2}+\frac{\partial^2 u}{\partial y^2}\right)+\nu_v\frac{\partial^2 u}{\partial z^2} \quad (1)$$

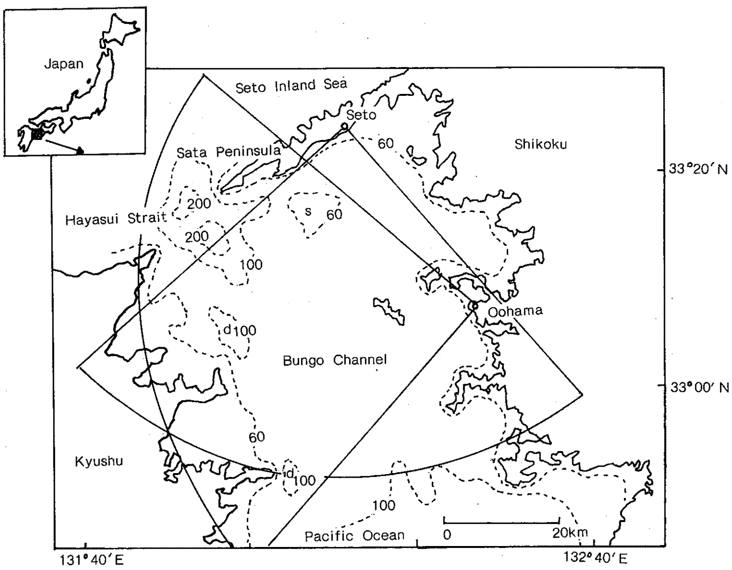

Fig. 1 Bungo Channel. Fan shows the coverage area of HF radar and the broken line with the figure the depth contour in meter.

$$\frac{\partial v}{\partial t}+u\frac{\partial v}{\partial x}+v\frac{\partial v}{\partial y}+w\frac{\partial v}{\partial z}+fu =-g\frac{\partial \eta}{\partial y}+\nu_h\left(\frac{\partial^2 v}{\partial x^2}+\frac{\partial^2 v}{\partial y^2}\right)+\nu_v\frac{\partial^2 v}{\partial z^2} \quad (2)$$

$$\frac{\partial \eta}{\partial t}+\frac{\partial}{\partial x}\int_{-h}^{\eta} u\,dz+\frac{\partial}{\partial y}\int_{-h}^{\eta} v\,dz=0 \quad (3)$$

Here x directs eastward, y northward, z upward from the mean sea surface, u, v, and w denote the velocity in x, y, and z directions, respectively, f(= 8.2×10^{-5} s^{-1} at 33.1°N) the Coriolis' parameter, g(= 980cm s^{-2}) the gravitational acceleralation, η the sea surface height from the mean sea surface, ν_h(=10^5 cm^2 s^{-1}) and ν_v(=10cm^2 s^{-1}) the horizontal and vertical eddy viscosities, respectively, and h the water depth.

The boundary conditions at the sea surface (z= 0) and at the bottom (z=−h) are given,

$$\frac{\partial u}{\partial z}=\frac{\partial v}{\partial z}=0,\ z=0 \quad (4)$$

$$u=v=w=0,\ z=-h \quad (5)$$

The normal velocity to the coast is zero. The observed amplitude and phase of M_2 constituent are given along the northern and southern open boundaries because it is the most dominant tidal constituent there (Yanagi, 1987) [6].

The numerical model is divided horizontally by 2km×2km and vertically 6 layers (1st; 0m to 10m, 2nd; 10m to 20m, 3rd; 20m to 30m, 4th; 30m to 50m, 5th; 50m to 75m and 6 th; 75m to bottom). Eqs.(1) to (3) are approximated by the finite difference and solved by the primitive method. The time step of the calculation is 30 seconds from the CFL condition. The velocity is zero at the beginning of the calculation. The steady oscillation is obtained four tidal cycles after the beginning of the calculation and the harmonic analysis of sea surface and current variations are carried out at every mesh point at the fifth tidal cycle.

The calculated co-tidal and co-range charts of M_2 tide are shown with the observed ones (Yanagi, 1987) [6] in Fig.2. The calculated results shown in Fig.2(a) and (b) well reproduce the observed ones (Yanagi, 1987) [6] shown in Fig.2(c).

The calculated maximum flood M_2 tidal current and maximum ebb one in the surface layer are shown in Fig.3 with the observed tidal current by HF radar (Yanagi et al., 1994) [5]. The M_2 tidal current amplitude is about 50cm s^{-1} in the central part of Bungo

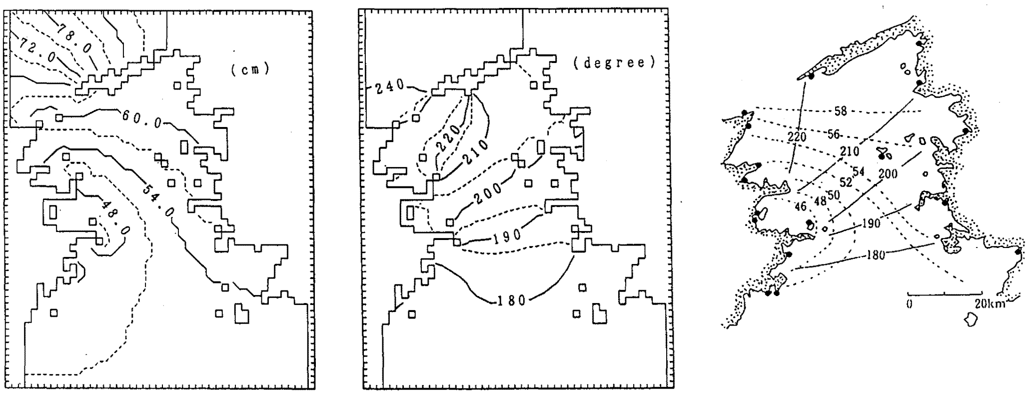

(a) (b) (c)

Fig. 2 Calculated M_2 tide amplitude (a), phase (b) and the observed co-tidal (full) and co-range (broken) lines (c), (Yanagi, 1987).

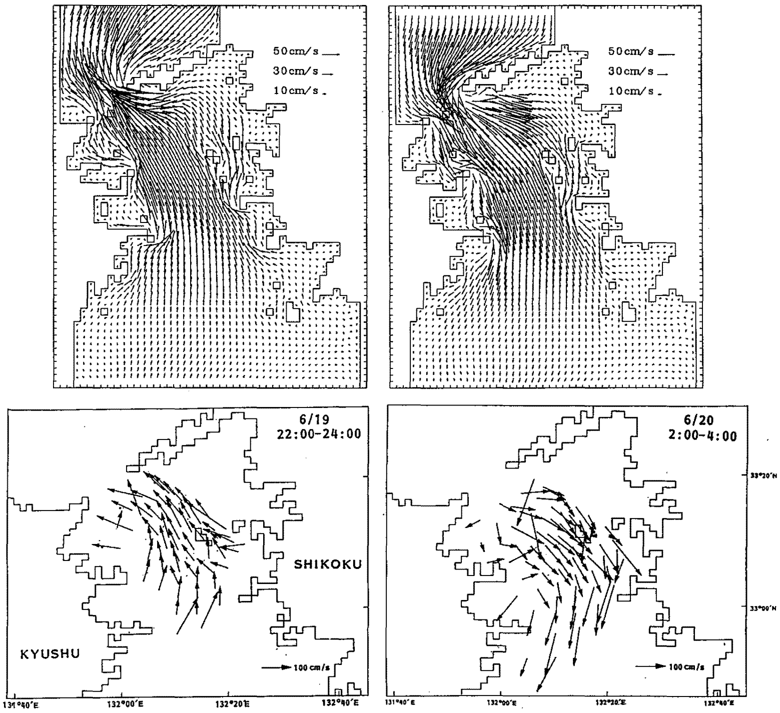

(a) (b)

Fig. 3 Calculated maximum flood tidal current at Hayasui Strait (upper a), maximum ebb (upper b), observed maximum flood (lower a) and maximum ebb (lower b) by HF radar (Yanagi et al., 1994).

Channel and over 100cm s^{-1} near Hayasui Strait. The current patterns of maximum flood and ebb are similar to those observed by HF radar though the current speeed by HF radar is larger than the calculated one because the observed tidal current includes other constituents than M_2 constituent. There is little vertical shear in the calculated tidal current.

The calculated tide-induced residual flow in the surface layer, which is obtained by averaging calculated tidal current over one-tidal cycle, is shown in Fig.4(a) and the tidal stress in the surface layer in Fig.4(b). Tidal stress (T_x, T_y) is calculated by the following formula,

$$T_x = \left< u\frac{\partial u}{\partial x} + v\frac{\partial u}{\partial y} + w\frac{\partial u}{\partial z} \right> \tag{6}$$

$$T_y = \left< u\frac{\partial v}{\partial x} + v\frac{\partial v}{\partial y} + w\frac{\partial v}{\partial z} \right> \tag{7}$$

Here < > denotes the averaging over one tidal cycle. Tide-induced residual flow is strong and its speed in about 10 – 15cm s^{-1} near Hayasui Strait where the tidal current amplitude is about 100cm s^{-1}. Tidal stress is large near the tip of headland with the magnitude of about 5×10^{-4}cm s^{-2} and small in the central part of Bungo Channel with the magnitude of about 10^{-4}cm s^{-2}. There is also little vertical difference in the tide-induced residual current and tidal stress.

3.2 Residual flow

Next we calculate the residual flow field in Bungo Channel by the diagnostic numerical calculation method with use of observed water temperature and salinity. The governing equations under Boussinesq and hydrostatic approximations are as follows,

$$\frac{\partial U}{\partial t} + U\frac{\partial U}{\partial x} + V\frac{\partial U}{\partial y} + W\frac{\partial U}{\partial z} - fV = -\frac{1}{\rho_0}\frac{\partial P}{\partial x} + \frac{\partial}{\partial x}\left(A_h\frac{\partial U}{\partial x}\right) + \frac{\partial}{\partial y}\left(A_h\frac{\partial U}{\partial y}\right) + \frac{\partial}{\partial z}\left(A_v\frac{\partial U}{\partial z}\right) + T_x \tag{8}$$

$$\frac{\partial V}{\partial t} + U\frac{\partial V}{\partial x} + V\frac{\partial V}{\partial y} + W\frac{\partial V}{\partial z} - fU = -\frac{1}{\rho_0}\frac{\partial P}{\partial y} + \frac{\partial}{\partial x}\left(A_h\frac{\partial V}{\partial x}\right) + \frac{\partial}{\partial y}\left(A_h\frac{\partial V}{\partial y}\right) + \frac{\partial}{\partial z}\left(A_v\frac{\partial V}{\partial z}\right) + T_y \tag{9}$$

$$P = \rho_0 g\eta + \rho_0\int_{-z}^{0} B\,dz \tag{10}$$

$$B = \frac{\rho_0 - \rho}{\rho_0} \tag{11}$$

$$\frac{\partial U}{\partial x} + \frac{\partial V}{\partial y} + \frac{\partial W}{\partial z} = 0 \tag{12}$$

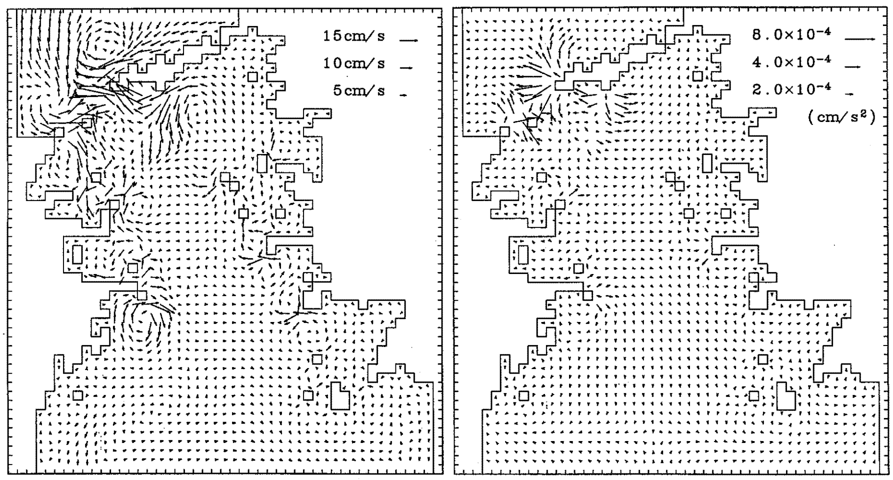

(a) (b)

Fig. 4 Calculated tide-induced residual flow (a) and tidal stress (b).

$$\frac{\partial T}{\partial t}+U\frac{\partial T}{\partial x}+V\frac{\partial T}{\partial y}+W\frac{\partial T}{\partial z}=\frac{\partial}{\partial x}\left(K_h\frac{\partial T}{\partial x}\right)+\frac{\partial}{\partial y}\left(K_h\frac{\partial T}{\partial x}\right)+\frac{\partial}{\partial z}\left(K_v\frac{\partial T}{\partial z}\right)+\gamma(T^*-T) \quad (13)$$

$$\frac{\partial S}{\partial t}+U\frac{\partial S}{\partial x}+V\frac{\partial S}{\partial y}+W\frac{\partial S}{\partial z}=\frac{\partial}{\partial x}\left(K_h\frac{\partial S}{\partial x}\right)+\frac{\partial}{\partial y}\left(K_h\frac{\partial S}{\partial y}\right)+\frac{\partial}{\partial z}\left(K_v\frac{\partial S}{\partial z}\right)+\gamma(S^*-S) \quad (14)$$

Here U, V, and W are x, y, and z components of residual flow, respectively, ρ the water density, ρ_0 the vertically averaged density, γ ($=0.5/\triangle t$, $\triangle t=30$ seconds) the nudging constant, T* and S* observed water temperature and salinity, A_h and A_v the horizontal and vertical eddy diffusivity, K_h and K_v the horizontal and vertical eddy diffusivity and are calculated from the tidal current amplitude on the basis of the mixing length theory.

$$A_h=\frac{2\alpha T}{\pi^2}u_{am}^2,\quad u_{am}=\sqrt{u_a^2+v_a^2} \quad (15)$$

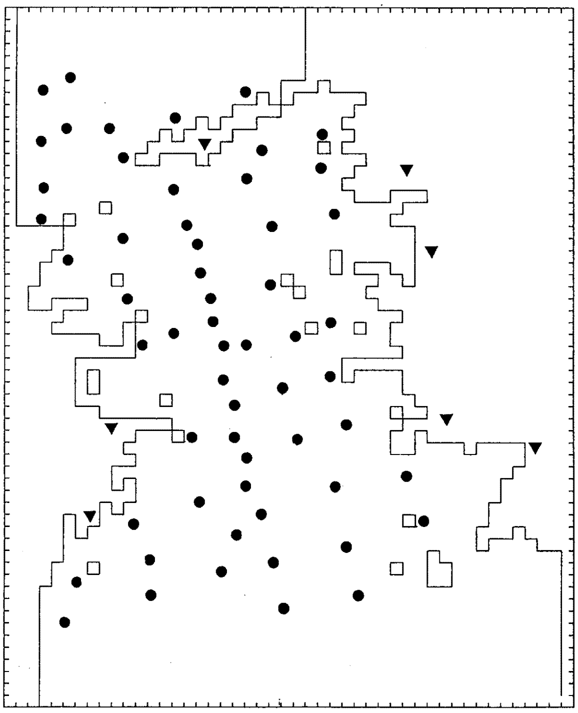

Fig. 5 Observation stations of water temperature and salinity (circle) and those of wind (triangle).

$$A_v=RA_h \quad (16)$$

$$K_h=0.1A_h \quad (17)$$

$$K_v=RK_h \quad (18)$$

Here α (=0.08) denotes the mixing ratio in one tidal cycle, T (=44700 sec) tidal period of M_2 constituent, u_a and v_a the M_2 tidal current amplitude in x and y directions, R ($=10^{-3}$) the aspect ratio of Bungo Channel, A_h varies between 10^5 cm^2 s^{-1} and 10^7 cm^2 s^{-1} in Bungo Channel from Eq.(15). Boundary conditions at the sea surface ($z=\eta$) and at the bottom ($z=-h$) are as follows,

at $z=\eta$

$$\rho_0\left(A_v\frac{\partial U}{\partial z},\ A_v\frac{\partial V}{\partial z}\right)=(\tau_x^s,\ \tau_y^s) \quad (19)$$

$$(\tau_x^s,\ \tau_y^s)=\rho_a C_a\left(W_x\sqrt{W_x^2+W_y^2},\ W_y\sqrt{W_x^2+W_y^2}\right) \quad (20)$$

at $z=-h$

$$\rho_0\left(A_v\frac{\partial U}{\partial z},\ A_v\frac{\partial V}{\partial z}\right)=(\tau_x^b,\ \tau_y^b) \quad (21)$$

$$(\tau_x^b,\ \tau_y^b)=\rho_0\gamma_b^2\left(U\sqrt{U^2+V^2},\ V\sqrt{U^2+V^2}\right) \quad (22)$$

Here ρ_a ($=0.0012$ g cm^{-3}) denotes the air density and C_a (=0.0013) the drag coefficient at the sea surface, γ_b^2 (=0.0026) the bottom drag coefficient, W_x and W_y the wind velocity in x and y directions, respectively. Along the coast and open boundaries, U =V=0.

Water temperature, salinity at the depths of 0, 5, 10, 20, 40, 60 m at 61 points shown in Fig.5 were observed by Ohita and Ehime Prefectures Fisheries Experimental Stations every early month. The water temperature and salinity at 61 stations in Bungo Channel on 23 June 1992 are estimated by linear interpolation from observed values in June and July 1992. Wind vector were observed every hour at seven stations on land shown in Fig.5 by the Meteorological Agency, Japan from 18 to 28 June 1992.

Water temperature and salinity are objectively interpolated in Bungo Channel with the hyperbolic function (Yanagi and Igawa, 1992) [7] and the interpolated water temperature, salinity and sigma-t in the surface, second, fourth and sixth layers are shown in

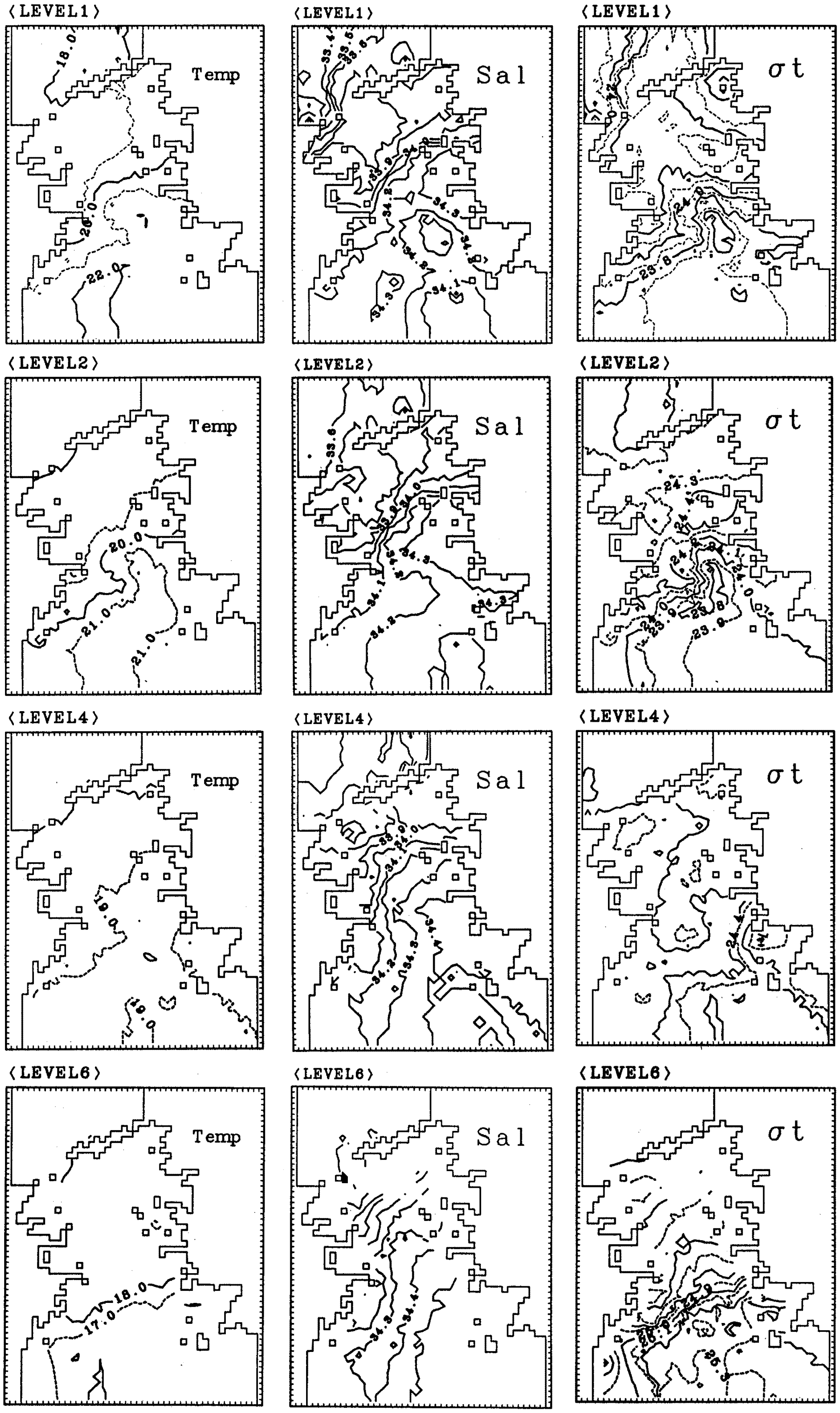

Fig. 6 Objectively interpolated water temperature, salinity and density (sigma-t) on 23 June 1992.

Fig.6. The Knudsen formula is used for the calculation of density (sigma-t) from water temperature and salinity. The cold, fresh and heavy water mass flows out along the western coast of Bungo Channel and the warm, saline and light water mass flows into along the eastern coast in the surface layer. On the other hand, the cold, saline and heavy water mass flows into the channel along the eastern coast in the bottom (sixth) layer.

The objectively interpolated sea surface wind averaged over the period of HF radar observation from 19 June to 27 June is shown in Fig.7. The weak northeastward wind with the speed of about 1.0m s^{-1} prevailed over Bungo Channel and this is the typical summer monsoon wind there.

Equations (8) to (14) are approximated by the finite difference. The forward difference scheme is adopted for the temporal acceralation term and the central difference scheme for the viscosity and diffusive terms. The upward difference scheme with the second order precision is adopted for the advection term. The model basin was at rest at the beginning of the calculation and the quasi-steady state was obtained about 20 hours after the beginning of the calculation. The calculated residual flow of both

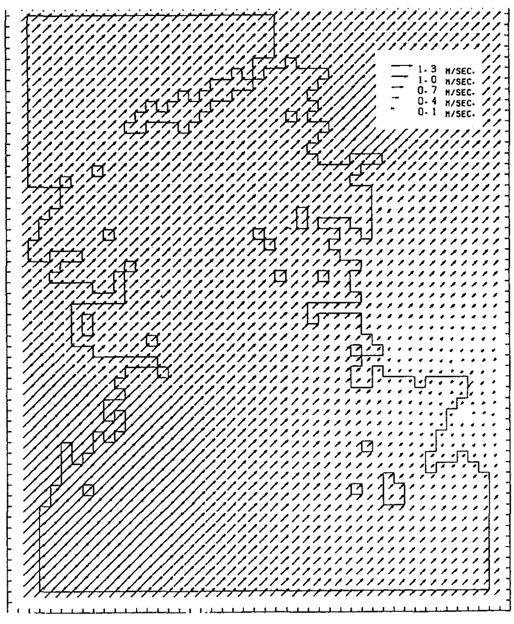

Fig. 7 Objectively interpolated sea surface wind averaged over 19 June and 27 June 1992.

models, with the tidal stress and without the tidal stress in Eqs. (8) and (9), are shown in Fig.8 (a) and (b), respectively. The southward residual flow with the speed of about 20cm s^{-1} is dominated in the surface layer at the northern and southern parts of Bungo Channel and a clockwise circulation in the bottom layer by the model results with the tidal stress as shown in Fig.8 (a). On the other hand, a clockwise circulation is developed in the surface layer at the northern part of Bungo Channel and the northward residual flow in the bottom layer by the model result without the tidal stress as shown in Fig. 8 (b).

The observed residual flow by HF radar shown in Fig.9 (a) shows that the southward residual flow with the speed of about 20cm s^{-1} is developed in the surface layer at the northern and southern parts of Bungo Channel. This suggests that the diagnostic numerical model with the tidal stress can reproduce correctly the observed residual flow field but that without the tidal stress cannot reproduce the observed result.

4. Discussion

The force balances of Eqs. (8) and (9) in x and y directions at the surface layer of both models along the north-south center line of Bungo Channel are shown in Fig.10. Main balance is established between the pressure gradient force and the Coriolis force in the case without the tidal stress. However the tidal stress is the largest and it balances to the pressure gradient force and the horizontal diffusion term in the northern part of Bungo Channel in the case with the tidal stress. In the case without the tidal stress, the westward residual flow in the upper layer of the central part of Bungo Channel is under the geostrophic balance between the southward pressure gradient force and the northward Coriolis force. This is due to that the fresh and light water mass exists in the upper layer around Hayasui Strait. On the other hand, in the case with the tidal stress, the residual flow directs southward in the upper layer of the central part of Bungo Channel because the southward tidal stress acceralates the southward residual flow and the main force balance is established among the tidal stress, the advection term and the

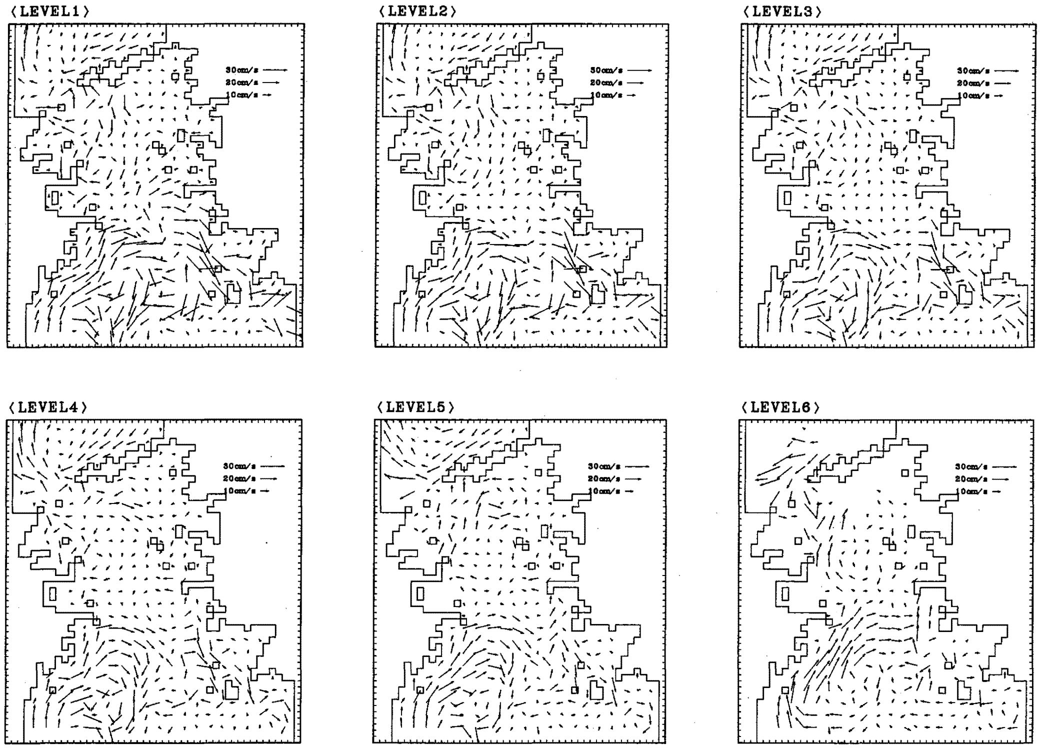

(a)

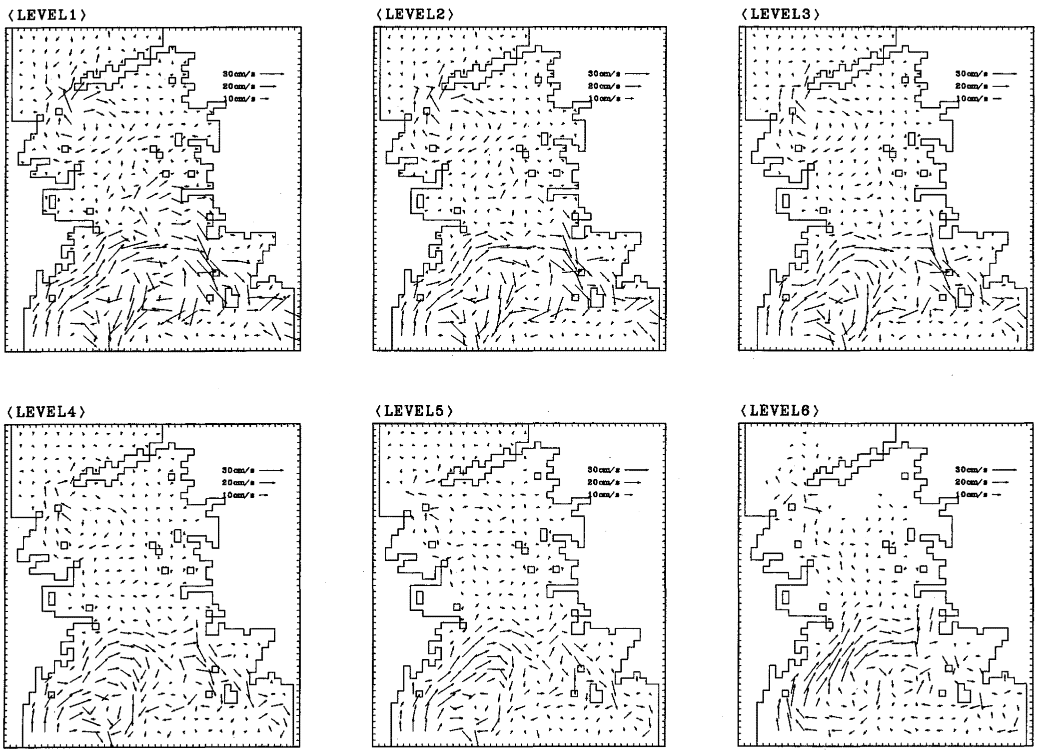

(b)

Fig. 8 Calculated residual flow by the model with the tidal stress (a) and that without the tidal stress (b).

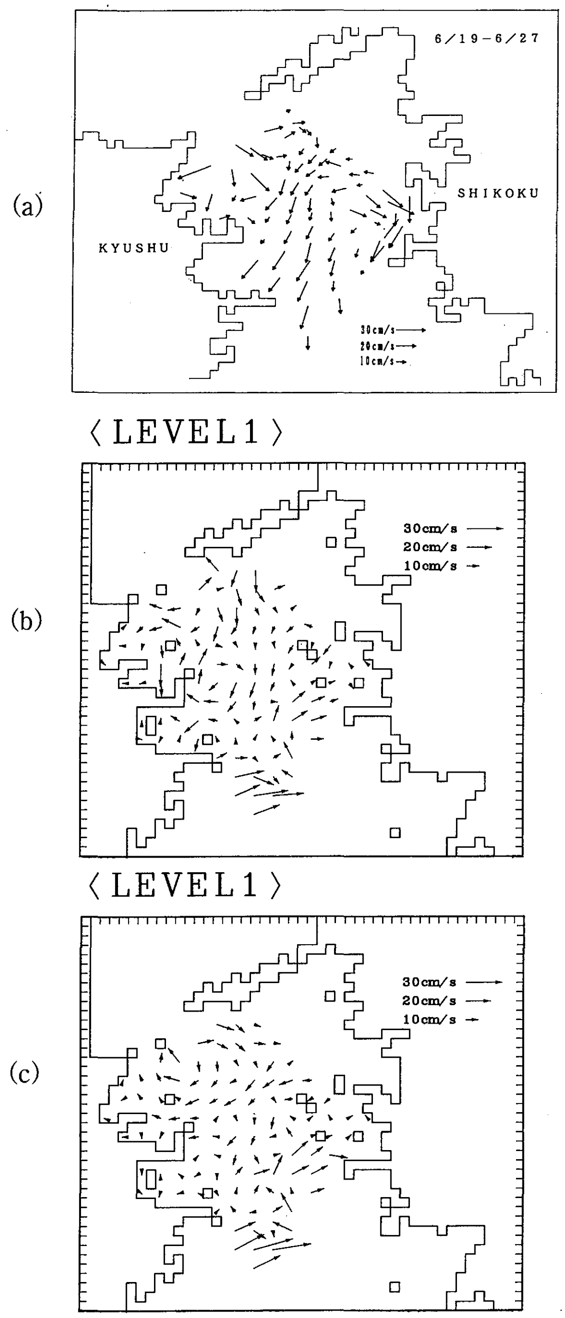

Fig. 9 Observed surface residual flow by HF radar (a), that by the model with the tidal stress (b) and that by the model without the tidal stress (c).

Coriolis force. Therefore the horizontal distributions of sea surface height are different between both cases with the tidal stress and without the tidal stress as shown in Fig.11; the mean sea surface is high around Hayasui Strait in the case without the tidal stress but it is high along the eastern and western coasts of Bungo Channel in the case with the tidal stress though the density distributions are the same in both cases as shown in Fig.6.

We can understand from these results that the tidal stress, whose magnitude is not so large as the pressure gradient force or the Coriolis force in the central part of the coastal sea, plays a very important role in the formation of residual flow field and we cannot reproduce correctly the residual flow field without the tidal stress in the diagnostic or prognostic numerical calculation of residual flow in the coastal sea where the tidal current is dominant.

Acknowledgements

The authors express their sincere thanks to Prof. H. Takeoka of Ehime University for his valuable discussion. This study is partly supported by the research fund defrayed from the Ministry of Education, Science, Culture and Sports, Japan.

References

[1] Backhaus, J.O. and D.Hainbucher A finite difference general circulation model for shelf seas and its application to low frequency variability on the North European Shelf. In"Three-dimensional models of marine and estuarine dynamics", ed. by J.C.J. Nihoul and B.M. Jamart, Elsevier, Amsterdam (1987), pp.221-244.

[2] Blumberg, A.F. and G.L. Mellor A description of a three-dimensional coastal ocean circulation model. In "Three-dimensional Coastal Ocean Models", ed. by C.N.K. Mooers, American Geophysical Union, Washington D.C. (1987), pp.1-16.

[3] Pohlmann, T. Predicting the thermocline in a circulation model of the North Sea-Part I: model description, calibration and verification. *Cont. Shelf Res.*, **16**(1996), 131-146.

[4] Lynch, D.R., J.T.C. Ippen, C.E.Naimie and F.E. Werner Comprehensive coastal circulation model with application to the Gulf of Maine. *Cont. Shelf Res.*, **16** (1996), 875-906.

[5] Yanagi, T., T.Miyazaki, Y.Ohno, Y.Hisaki, A. Nadai and H.Kuroiwa Variability of the dynamical state of Bungo Channel VI-HF radar observation. *Memoirs of the Faculty of Engineering, Ehime Univ.*, **VIII**(1994), 333-337 (in Japanese with English

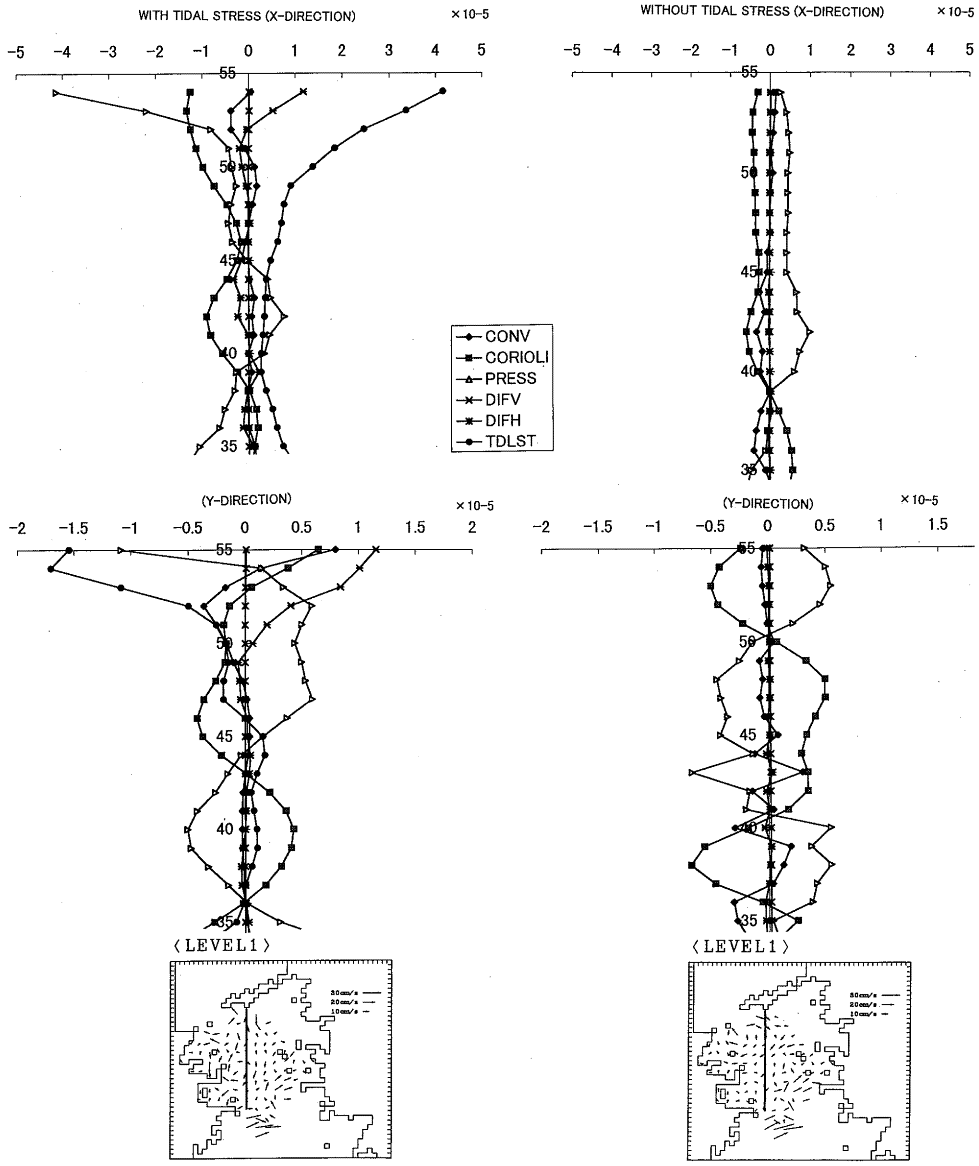

(a) (b)

Fig. 10 Calculated force balances in x and y directions along the center line by the model with the tidal stress (a) and that without the tidal stress (b).

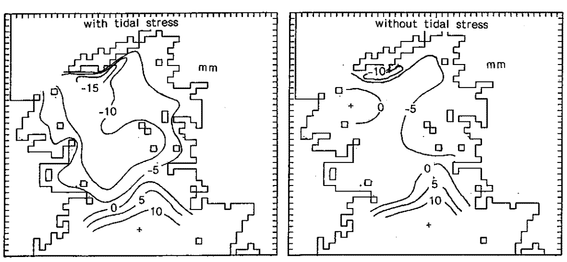

(a) (b)

Fig. 11 Calculated sea surface elevation by the model with the tidal stress (a) and that without the tidal stress (b).

abstract and captions).

[6] Yanagi, T. Kelvin wave reflection with phase lag in Bungo Channel. *J. Oceanogr. Soc. Japan*, **43** (1987), 377-382.

[7] Yanagi, T. and S.Igawa Diagnostic numerical model of residual flow in the coastal sea—An example of Suo-Nada and Iy-Nada-. *Bulletin on Coastal Oceanography*, **30** (1992), 108-115 (in Japanese with English abstract and captions).